PCCP

ROYAL SOCIETY OF CHEMISTRY

PAPER

View Article Online
View Journal | View Issue

Cite this: *Phys. Chem. Chem. Phys.*, 2026, **28**, 3204

High-entropy FeCoNiCrCe layered double hydroxides by facile pulse current electrodeposition as high performance electrocatalysts for the oxygen evolution reaction

Xinyu Yang and Qianqiao Chen *

A high-entropy strategy can promote the electrocatalytic activity of catalysts through a synergistic electronic environment. In this work, a high-entropy FeCoNiCrCe LDH was *in situ* constructed on a nickel foam substrate *via* facile pulse current (PC) electrodeposition at room temperature in just 20 minutes. This electrode outperforms its counterpart prepared by direct current (DC) electrodeposition, with a low overpotential of 215 mV at 10 mA cm^{-2} and a small Tafel slope of 45.15 mV dec^{-1}. Notably, it exhibited remarkable stability during a 7-day chronopotentiometric test at 50 mA cm^{-2}. The enhancements arise not only from the synergistic effect of five-metal composition, but more importantly, from the microstructural advantages of the PC-prepared electrode, which are revealed from a novel perspective by comparison with its DC-prepared counterpart electrode. which are revealed from a novel perspective by comparison with its DC-prepared electrode, which served as the counterpart. The optimized surface morphology with uniform element distribution and similar content by PC electrodeposition enables more effective electronic structure modulation of the active sites by Cr and Ce in the local micro-region. Moreover, the near-equal element composition in FeCoNiCrCe is conducive to increasing the configuration entropy, making the high-entropy stabilization effect more pronounced, thereby leading to enhanced structural stability and OER durability compared to the DC counterpart.

Received 20th October 2025,
Accepted 28th December 2025

DOI: 10.1039/d5cp04024h

rsc.li/pccp

1. Introduction

Water electrolysis is a promising technology for hydrogen production, yet the oxygen evolution reaction (OER) poses a challenge to energy conversion efficiency due to its sluggish four-electron transfer mechanism and theoretical potential of up to 1.23 V.[1–3] Current research focuses on two approaches to address this challenge: replacing the anodic OER with thermodynamically more favourable oxidation reactions such as the glucose oxidation reaction (GOR)[4,5] and the urea oxidation reaction (UOR);[6,7] or developing more efficient OER catalysts.[8–10] While noble metals and their derivatives, such as Ru and RuO_2, currently represent the benchmark catalysts for commercial applications, their large-scale applications are hindered by high cost, scarcity, and insufficient durability in alkaline media.[10–12] These limitations have motivated the exploration of transition metal alternatives combining cost-effectiveness with comparable catalytic performance. Recent research has shown that modifying the electronic structure can improve the catalytic activities effectively,[13] and using high-entropy materials (HEMs) provides a promising approach for such optimization.[6] HEMs containing five or more homogeneously distributed elements,[14,15] have recently garnered significant interest as OER catalysts due to their tailorable coordination geometries, tunable electronic configurations, and inherent multivalent character arising from coexisting elemental oxidation states.[15,16]

Layered double hydroxides (LDHs) are regarded as promising OER electrocatalysts, owing to their compositional tunability and high specific surface area. However, they still suffer from inherent limitations including poor conductivity and structural degradation induced by metal ion leaching.[17,18] Moreover, their OER performance under high-current-density and long-term stability remain inadequate for industrial requirements due to the irreversible side reactions during the reaction process.[19,20] Introducing the concept of high-entropy into LDHs offers a viable solution to the above constraints. For example, Li *et al.* reported a seven-element high-entropy LDH which exhibited excellent alkaline durability, showing a potential increase less than 5% after 48-h test at a high current density of 250 mA cm^{-2}.[20] Currently, the synthesis of high-

School of Chemistry and Chemical Engineering, Nanjing University of Science and Technology, Nanjing, 210094, China. E-mail: cqq@njust.edu.cn

entropy LDHs relies predominantly on a hydrothermal method,[18,21,22] which involves extended processing time and heat. Although heating-free methods have been developed, those approaches are still time-consuming.[23,24]

Transition metal elements such as Fe, Co, and Ni are widely recognized as active sites for the OER.[13,25,26] Incorporating metal elements with high-valence states (such as Mn, Cr, Ru and W) has positive effects on improving the catalyst morphology and increasing catalytic active sites.[6,20] Rare earth elements with 4f valence orbitals, for example, Ce, can optimize the electron distribution of transition metal elements and thus enhance the catalytic performance.[27,28] Based on the above, Fe, Co, Ni, Cr, and Ce are selected as the five metal elements for synthesizing a high-entropy FeCoNiCrCe LDH, which is expected to be a high performance electrocatalyst for the OER.

Electrodeposition has emerged as a fabrication method for nanomaterials, since the difference in coordination ability or reduction potential among different metal ions can be overcome at high overpotential.[9,29] Moreover, this method could achieve nanoparticles with different shapes and sizes by modulating electrodeposition parameters.[30,31] Electrodeposition can be driven by various electrical modes, such as static potential,[9] cyclic voltammetry,[32] direct current (DC),[33,34] and pulse current (PC).[35] Although DC electrodeposition has been used in various engineering applications, PC electrodeposition has recently garnered increased interest due to the improved plating efficiency and coating quality such as smoothness, hardness and mechanical properties, which benefits from superior current distribution and enhanced ion mass transfer.[35,36] Chang *et al.* developed a FeCoNiMnW high-entropy alloy on carbon paper *via* PC electrodeposition to use as an excellent bifunctional catalyst for acidic water electrolysis. It exhibits an ultra-low overpotential of 15 mV for the HER and a usable overpotential of 512 mV for the OER, both at 10 mA cm^{-2}.[37]

Herein, a facile PC electrodeposition method was utilized to *in situ* construct a high-entropy FeCoNiCrCe LDH (denoted as FeCoNiCrCe) on a nickel foam substrate at room temperature. This rapid strategy achieves binder-free electrodes in just 20 minutes, effectively avoiding active sites clogged by polymeric additives and performance deterioration caused by catalyst powder peeling off the substrate during sustained electrolysis.[2,38] The FeCoNiCrCe electrode not only outperforms medium-/low-entropy LDHs obtained by the same PC method but is also superior than its DC-prepared counterpart in OER activity, achieving a low overpotential of 215 mV at 10 mA cm^{-2} and a small Tafel slope of 45.15 mV dec^{-1}. Notably, it exhibited remarkable stability during a 7-day chronopotentiometric test at 50 mA cm^{-2} with only a 0.2% potential increase. In this work, the microstructural advantages of the electrode prepared by PC electrodeposition have been revealed by comparing with the DC-prepared electrode. The optimized surface morphology with uniform element distribution of FeCoNiCrCe enables more effective electronic modulation of the active sites by the surrounding Cr and Ce, thus improving OER activity. Moreover, the near-equal elemental content of the PC-prepared electrode facilitates an increase in configuration entropy, making the high-entropy stabilization effect more pronounced, which helps suppress metal ion leaching, thereby leading to enhanced structural stability and OER durability compared to its DC counterpart.

2. Experimental

2.1 Reagents and materials

Hydrochloric acid (HCl, AR), acetone (CH_3COCH_3, AR), ethanol (C_2H_5OH, AR), iron(III) nitrate nonahydrate ($Fe(NO_3)_3{\cdot}9H_2O$, AR), cobalt(II) nitrate hexahydrate ($Co(NO_3)_2{\cdot}6H_2O$, AR), nickel(II) nitrate hexahydrate ($Ni(NO_3)_2{\cdot}6H_2O$, AR), chromic(III) nitrate nonahydrate ($Cr(NO_3)_3{\cdot}9H_2O$, AR), cerium(III) nitrate hexahydrate ($Ce(NO_3)_3{\cdot}6H_2O$, AR) and ammonium fluoride (NH_4F, AR) were provided by Sinopharm Chemical Reagent Co. Ltd (Shanghai, China). None of them were further processed. Nickel foam (NF) was purchased from Kunshan City Guangjiayuan electronic materials.

2.2 Synthesis of LDH electrodes

The synthesis of high-entropy FeCoNiCrCe LDH was taken as an example. First, the NF (1 cm × 2 cm) was ultrasonically cleaned with 3 M HCl, CH_3COCH_3, C_2H_5OH, and deionized water in order to remove the surface oxide layer and to activate. Then, 0.6 mM $Fe(NO_3)_3{\cdot}9H_2O$, $Co(NO_3)_2{\cdot}6H_2O$, $Ni(NO_3)_2{\cdot}6H_2O$, $Cr(NO_3)_3{\cdot}9H_2O$, $Ce(NO_3)_3{\cdot}6H_2O$, and 4 mM NH_4F were dissolved in 100 mL of deionized water. The mixture was stirred until it became completely transparent and used as the electrolyte solution. Using an Ivium-N-Stat electrochemical workstation, a standard three-electrode system was employed for the electrodeposition of FeCoNiCrCe, with the treated NF as the working electrode, a carbon rod as the counter electrode, and a Hg/HgO electrode as the reference electrode. The PC electrodeposition method was performed with a current density of 100 mA cm^{-2} with an on/off cycle of 15/5 s 60 times (20 min) at room temperature. After the electrodeposition process, the electrode was dried under vacuum at 60 °C. For comparison, quaternary, ternary, and binary LDH catalysts were prepared under identical PC conditions and designated as FeCoNiCr, FeCoNi, and FeCo, respectively. To investigate the effects of different current modes on the microstructure and catalytic performance of the sample, the DC electrodeposition method was performed for 20 min with a current density of 100 mA cm^{-2}, and the corresponding electrode is named FeCoNiCrCe-DC.

2.3 Characterization

To investigate the molecular and crystal structure of FeCoNiCrCe, a titanium mesh was also used as the working electrode (given the strong adhesion between the LDH particles and the NF substrate), and the same PC electrodeposition operation was carried out. The LDH particles were detached from the titanium mesh by ultrasonic treatment, collected by centrifugation and vacuum dried. Fourier transform infrared spectroscopy (FT-IR, Thermo Fisher Nicolet iS10) was performed in a

range of 4000–400 cm^{-1}. X-ray diffraction (XRD, Bruker D2 Phaser) with Cu Kα irradiation was used to examine the crystal structure. The morphology of the as-prepared electrodes was investigated using scanning electron microscopy (SEM, HITACHI Regulus 8100) at an acceleration voltage of 2 kV combined with energy dispersive spectroscopy (EDS). Transmission electron microscopy (TEM, JEOL JEM 2100) was performed at 200 kV. X-ray photoelectron spectroscopy (XPS, Thermo Fisher Scientific K-Alpha) was used to examine the surface oxidation sate of the electrodes. All XPS spectra were corrected by using the C 1s line at 284.8 eV, and the curve fitting and background subtraction were accomplished. Elemental distribution was studied with element mapping images. The elemental composition and content were determined by inductively coupled plasma optical emission spectroscopy (ICP-MS, Agilent 700).

2.4 Electrochemical measurements

All electrochemical measurements were carried out on an Ivium-N-Stat electrochemical workstation at room temperature. The as-prepared electrodes were applied as the working electrode directly (work surface area: 1 cm × 1 cm), the counter electrode was a carbon rod, and a Hg/HgO electrode was used as the reference electrode. One molar KOH solution was used as the electrolyte. OER performance was measured by performing linear sweep voltammetry (LSV, scan rate of 2 mV s^{-1}). Unless otherwise stated, all potentials in this work were converted to reversible hydrogen electrode (RHE) using the equation. $E_{RHE} = E_{Hg/HgO} + 0.059pH + 0.098$. All LSV results were compensated with a 95% iR correction. The Tafel slopes were calculated by converting the LSV diagram. The mass activity was determined using the following equation: $j_m = j/m$, where j represents the measured current density at a potential of 1.45 V, and m denotes the catalyst loading, which was calculated by measuring the mass difference of the NF before and after the electrodeposition. Electrochemical impedance spectroscopy (EIS) tests were performed in the range of 0.1 MHz to 0.1 Hz with an amplitude of 5 mV at 0.6 V (*vs.* $E_{Hg/HgO}$). The chronopotentiometry (CP) test was performed at a current of 50 mA cm^{-2}. The electrochemical active surface area (ECSA) was calculated from double-layer capacitance (C_{dl}), and the C_{dl} was obtained from cyclic voltammetry (CV) plots with different scan rates (20, 40, 60, 80, 100 mV s^{-1}) from 0.04 V to 0.14 V against the RHE. The ECSA was obtained using the equation: ECSA = C_{dl}/C_s, where C_s is the specific capacitance. The used value for C_s is 0.04 mF cm^{-2} in 1 M KOH. The roughness factor (R_f) was calculated by dividing the ECSA by the geometric area of the working electrode.

3. Results and discussion

The preparation of FeCoNiCrCe is depicted in Fig. 1a. As shown in Fig. S1, the FTIR spectra reveal the presence of the carbonate anion (CO_3^{2-}) in the interlayers, as suggested by the characteristic peak located at 1384 cm^{-1},[39] and a small absorption peak at 1060 cm^{-1}.[18] Two peaks at 668 and 518 cm^{-1} correspond to the metal–oxygen (M–O) bonds.[39] The broadened peak centered at 3420 cm^{-1} and peaks around 1600 cm^{-1} are attributed to the stretching vibrations of O–H groups on the surface and absorbed water, respectively.[18,21] The crystal structures were determined by XRD. As shown in Fig. S2, the diffraction peaks of the FeCo LDH could be attributed to the CoFe LDH (PDF#50-0235).[40] Three peaks, located at 23.4, 36.6 and 43.3°, could be attributed to the reflection of the (0 0 6), (1 0 4) and (1 0 7) lattice planes, respectively. The incorporation of Ni, Cr, and Ce atoms reduces the intensities of diffraction peaks, indicating crystallinity degradation. Furthermore, there is an obvious negative shift of the (0 0 6) plane of FeCoNiCrCe, suggesting that Ce atoms, which have the largest atomic radius among the chosen elements, lead to an increase in the interplanar spacing and lattice distortion. This disordered structure may offer a large accessible surface area, accelerating the OER by modifying the electronic structure in active sites.[41,42]

SEM characterization reveals the morphological difference under the PC and DC electrodeposition. The FeCoNiCrCe-DC electrode displays a cauliflower-like surface,[30] composed of aggregated particles (Fig. 1b). In contrast, the PC-prepared electrode exhibits a furry surface morphology (Fig. 1a), which is expected to enhance OER activity due to the potentially increased specific surface area and exposed catalytic active sites.[43] Moreover, the FeCoNiCrCe electrode demonstrates a superior surface elemental composition compared to its DC counterpart. The surface element content analysis using SEM (Fig. 1c) reveals that the surface of FeCoNiCrCe-DC is predominantly composed of Ni, while FeCoNiCrCe exhibits a more near-equal surface composition. The bulk composition and the content of each metal element in FeCoNiCrCe were further quantified by ICP-MS. The contents of Fe, Co, Ni, Cr and Ce in the total metal contents are 19.35%, 20.66%, 23.7%, 18.62% and 17.67%, respectively. The similar metal element content contributes to increasing the configuration entropy of FeCoNiCrCe, and thus has a positive effect on its OER performance.[20]

It can be inferred that the surface morphology is related to the applied current mode. Under the DC conditions, sustained metal ion consumption induces concentration polarization and hydrogen evolution as a side reaction, while the PC electrodeposition utilizes intermittent current cycles to allow ionic replenishment during off-time periods. This periodic recovery effectively suppresses the generation of hydrogen while maintaining deposition efficiency.[35] Consequently, the PC-prepared electrode exhibits a better surface morphology and element composition. The TEM analysis of FeCoNiCrCe (Fig. 1e–g) reveals a hybrid crystalline-amorphous structure, with amorphous zones (Region A, Fig. 1e) and a crystalline region (Region B, Fig. 1g). The amorphous morphology in Region A originates from random distribution of multi-metallic atoms with different radii, creating lattice distortion in the high-entropy LDH. The measured 0.2 nm lattice spacing in Region B corresponds to the (1 0 4) plane of CoFe LDH (PDF#50-0235), consistent with XRD results. Such a unique crystalline-amorphous structure benefits catalytic activity since the crystalline-phase accelerates the mass diffusion and the charge transfer, while the

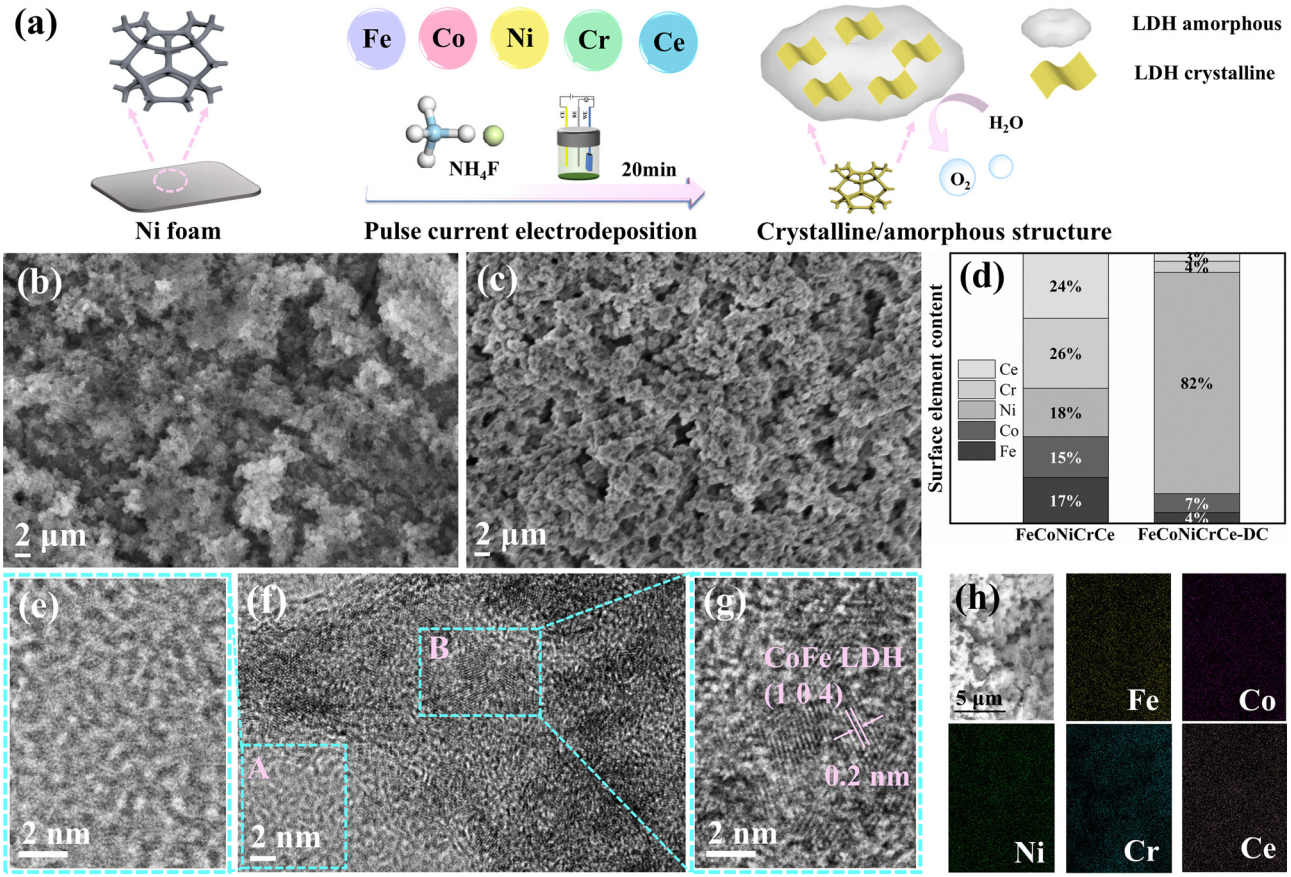

Fig. 1 (a) Schematic illustration of the preparation of FeCoNiCrCe. SEM images of (b) FeCoNiCrCe and (c) FeCoNiCrCe-DC. (d) Surface element content of FeCoNiCrCe and FeCoNiCrCe-DC. (e)–(g) TEM images of FeCoNiCrCe. (h) Corresponding element mapping images.

uncoordinated sites of the amorphous-region offer abundant valid active sites for the OER.[44,45] The element mapping images (Fig. 1h) confirm the even distribution of each element on the FeCoNiCrCe surface. XRD, FTIR and TEM analyses prove that FeCoNiCrCe is mainly composed of the LDH structure, and ICP-MS proved that the composition of each element is between 5% and 35%. The above results collectively validate that FeCoNiCrCe meets the requirements for a HEM.

XPS was performed to further investigate the oxidation state and electron coupling interaction of FeCoNiCrCe, FeCoNiCrCe-DC and FeCoNi. The survey spectrum (Fig. S3) confirms the presence of Fe, Co, Ni, Cr, Ce, O, and C elements in FeCoNiCrCe. The high-resolution Fe 2p XPS spectra are shown in Fig. 2a. In FeCoNi, two peaks of Fe $2p_{3/2}$ and Fe $2p_{1/2}$ are located at 712.4 and 725.1 eV, respectively. The peak at 717.6 eV is a satellite peak (denoted as "Sat."). The Fe $2p_{3/2}$ peak can be deconvoluted into a Fe^{2+} peak at 705.6 eV and a Fe^{3+} peak at 712.2 eV. But with the addition of Cr and Ce, Fe^{2+} disappears and there is only Fe^{3+}.[21,46] Fig. 2b reveals the coexistence of Co^{3+} and Co^{2+} in the ternary sample and quinary samples. For FeCoNiCrCe, peaks of Co $2p_{3/2}$ and Co $2p_{1/2}$ are seen at 780.9 and 796.8 eV, respectively. Two satellite peaks are found at 785.7 and 802.9 eV.[29] Compared to FeCoNi and FeCoNiCrCe-DC, the Co 2p peaks for FeCoNiCrCe exhibit a slight positive shift. In the high-resolution Ni 2p spectrum of FeCoNiCrCe (Fig. 2c), two peaks at 855.3 and 873.2 eV correspond to Ni $2p_{3/2}$ and Ni $2p_{1/2}$, respectively, with satellite peaks at 861.2 and 879.3 eV.[47] It can be seen that Ni^{2+} (855.4 and 873.0 eV) is dominant in FeCoNi, however, the fractions of Ni^{3+} in FeCoNiCrCe (856.3 and 874.6 eV) increase. Despite a higher surface Ni content on FeCoNiCrCe-DC (Fig. 1c), the FeCoNiCrCe surface offers a greater density of Co^{3+} and Ni^{3+} species, which are regarded as the active sites for the OER.[13,26] A monovalent state is found in the Cr 2p spectra (Fig. 2d). Two peaks at 577.3 and 587.0 eV can be attributed to Cr $2p_{3/2}$ and Cr $2p_{1/2}$ of Cr^{3+}, respectively.[6] The XPS spectrum of Ce 3d (Fig. 2e) exhibits two main peaks at 884.1 and 902.4eV attributable to Ce^{4+}, along with peaks at 887.1 eV and 905.7 eV attributed to Ce^{3+} species.[26] In the O 1s spectrum (Fig. 3f) of FeCoNiCrCe, metal–oxygen (M–O), metal–hydroxyl (M–OH), and surface adsorbed water (H–O–H) peaks can be found at 530.7, 531.5, and 533.7 eV, respectively,[20] where M represents the metal in the sample. The fractions of M–O increase with the introduction of metals into FeCoNiCrCe, suggesting the increased metal–oxygen covalency.[21]

Electrochemical tests were conducted using a traditional three-electrode cell in 1 M KOH. Linear sweep voltammetry (LSV) measurements on samples prepared by different methods were performed first to study the effect of current mode on the OER activity. The onset potential is defined as the potential required to reach a current density of 1 mA cm^{-2}.[48] As shown in

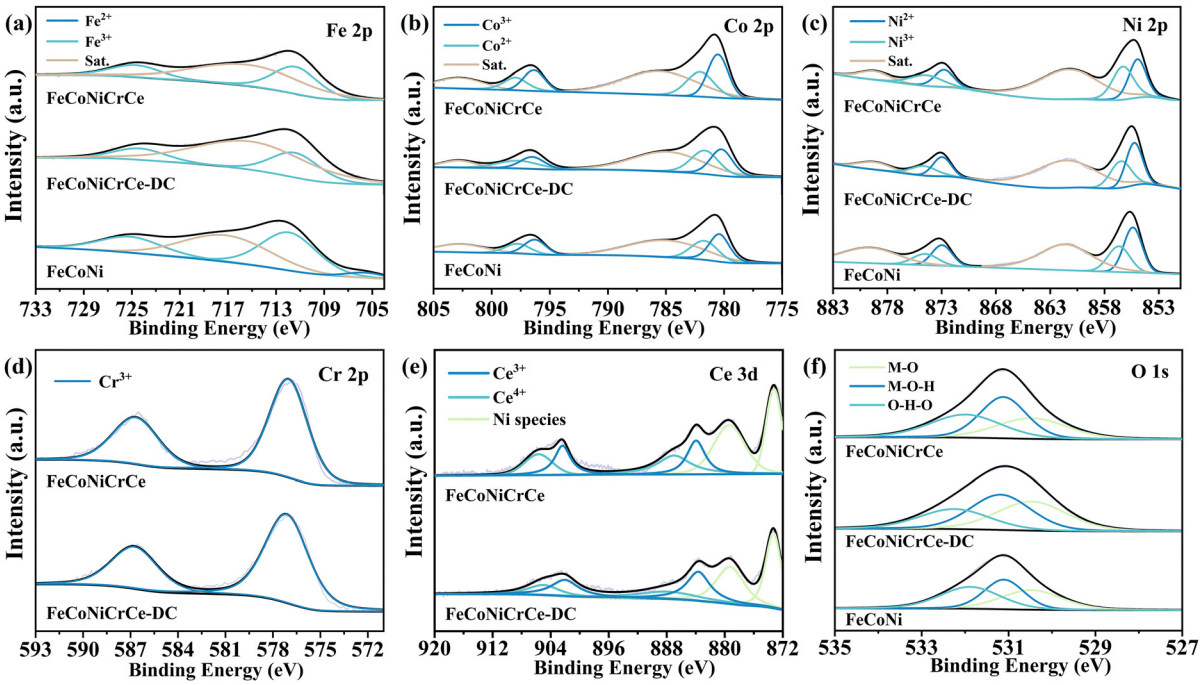

Fig. 2 High-resolution XPS spectra of (a) Fe 2p, (b) Co 2p, (c) Ni 2p, (d) Cr 2p, (e) Ce 3d, and (f) O 1s.

Fig. S4a, the onset potentials for FeCoNiCrCe and FeCoNiCrCe-DC are 1.428 V and 1.434 V, respectively, with a difference of 6 mV. Moreover, FeCoNiCrCe exhibits better OER activity at high current density compared to the DC counterpart. The Tafel slope provides insight into the reaction kinetics of the catalyst.[49] FeCoNiCrCe exhibits a smaller Tafel slope of 45.15 mV dec^{-1} while that of FeCoNiCrCe-DC is 71.55 mV dec^{-1}, suggesting the superior OER kinetics of FeCoNiCrCe (Fig. S4b). Electrochemical impedance spectroscopy (EIS) can be used to determine the charge transfer resistance (R_{ct}) of the working electrode. The Nyquist plots are depicted in Fig. S4c. The R_{ct} values of FeCoNiCrCe and FeCoNiCrCe-DC are 0.35 Ω and 0.45 Ω, respectively. A reduced R_{ct} facilitates a higher charge transfer rate. The Tafel slope and EIS data collectively demonstrate the reason for the better OER activity of FeCoNiCrCe. The intrinsic activity of electrodes prepared in different current modes was obtained from multi-rate cyclic voltammetry (CV) tests in the non-faradaic region, and the corresponding double-layer capacitance (C_{dl}) and electrochemical active surface area (ECSA) were calculated. As shown in Fig. S4f, the C_{dl} of FeCoNiCrCe is four times that of FeCoNiCrCe-DC, suggesting a lager ECSA, which is consistent with SEM analysis. Moreover, the mass activity of two electrodes was calculated at an applied potential of 1.45 V (*vs.* RHE). The mass activity values for FeCoNiCrCe and FeCoNiCrCe-DC are 1.14 and 0.59 A g^{-1}, respectively. Both C_{dl} and mass activity indicate that FeCoNiCrCe has higher intrinsic activity.

Due to the advantages in producing samples with better surface composition and enhanced OER activity and kinetics, samples fabricated by the same PC electrodeposition method and a piece of pretreated pure NF were selected for further OER performance comparison studies. As presented in Fig. 3a, the pure NF exhibits very low OER activity. The electrodeposition of the catalyst onto it markedly boosts the catalytic activity. FeCoNiCrCe exhibits outstanding performance for OER catalysis, since it requires only 1.445 V to reach a current density of 10 mA cm^{-2}. Additionally, it maintains a remarkably low overpotential of 300 mV even when the current density reaches 500 mA cm^{-2}, confirming the ability to sustain high catalytic efficiency at high current density. The overpotential is an important parameter for measuring catalytic efficiency.[50] Fig. 3b presents a comparison of the overpotentials calculated at different current densities for the LDH electrodes. Introducing different metals progressively decreases the overpotential from bimetal FeCo LDH to high-entropy LDH, and FeCoNiCrCe requires the lowest overpotentials across the tested range. Recent studies have also reported that multi-component catalysts outperform single-component or binary/ternary systems.[51,52] This enhancement stems from the synergistic interaction among the component elements, which optimizes the electronic structure of the multi-metallic system due to their diverse valence states.[53] Therefore, the catalyst possesses a broader range of possible adsorption energies for reaction intermediates within the working potential window, leading to enhanced OER catalytic activity.[21,38]

The reaction kinetics of the electrodes were characterized by the Tafel slope analysis (Fig. 3c). FeCoNiCrCe exhibits the lowest Tafel slope of 45.15 mV dec^{-1} and is smaller than those of FeCoNiCr (55.91 mV dec^{-1}), FeCoNi (68.42 mV dec^{-1}), FeCo (88.3 mV dec^{-1}) and pure NF (123.35 mV dec^{-1}), which is consistent with the fastest current density increase of FeCoNiCrCe, indicating its fastest electron transfer rate and superior OER kinetics. The kinetics at the interface between the catalyst and the electrolyte were analyzed using EIS. The Nyquist plots

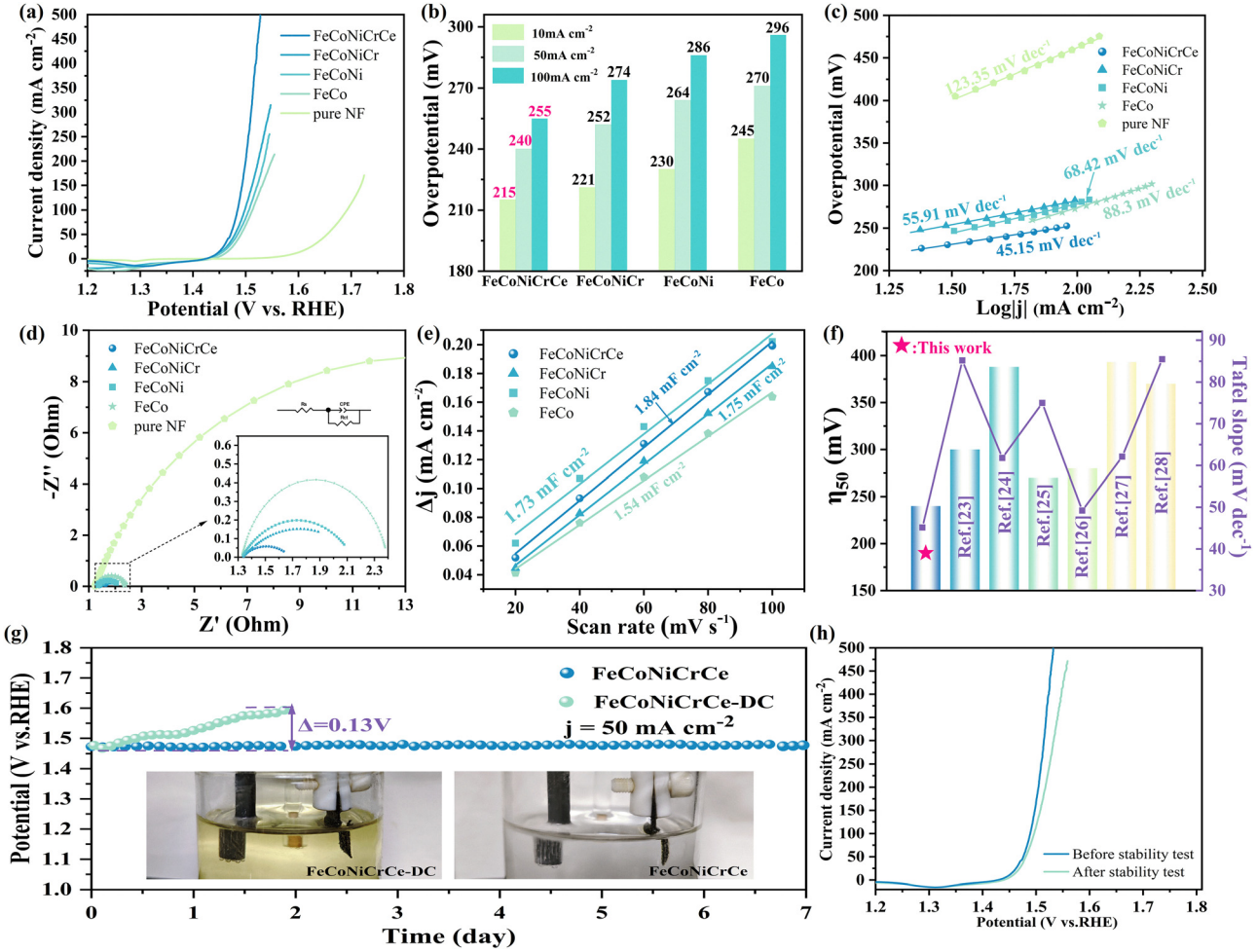

Fig. 3 (a) LSV curves for the OER activity of the PC-prepared electrodes and pure NF. (b) Comparison of overpotential at different current densities of PC-prepared electrodes. (c) Tafel slopes and (d) Nyquist plots of the PC-prepared electrodes and pure NF (inset: equivalent circuit model). (e) The double-layer capacitance for the OER of the PC-prepared electrodes. (f) Comparison of the overpotentials at 50 mA cm^{-2} and Tafel slopes of the reported catalysts. (g) Chronopotentiometric test curves of FeCoNiCrCe and FeCoNiCrCe-DC for the OER under a current density of 50 mA cm^{-2}. (h) LSV curves of FeCoNiCrCe before and after the stability test.

are shown in Fig. 3d, and the corresponding equivalent circuit model (inset of Fig. 3d) consists of the electrolyte resistance (R_s), charge transfer resistance (R_{ct}), and constant phase element (CPE). The high-entropy LDH has the minimal R_{ct}, about 0.35 Ω, indicating its fastest charge-transfer rate. The Tafel slope and EIS data collectively elucidate the reason behind the high OER activity of the high-entropy FeCoNiCrCe LDH.

Multi-rate CV tests were also performed to further investigate the intrinsic activity of the catalysts (Fig. S5). As revealed in Fig. 3e, the C_{dl} of FeCoNiCrCe is 1.84 mF cm^{-2}, which is higher than those of FeCoNiCr (1.75 mF cm^{-2}), FeCoNi (1.73 mF cm^{-2}), and FeCo (1.54 mF cm^{-2}). This demonstrates that FeCoNiCrCe exposes more active sites, as the ECSA is proportional to the C_{dl}.[18] The ECSA of FeCoNiCrCe, FeCoNiCr, FeCoNi, and FeCo is 46, 43.75, 43.25, and 38.5, respectively. The high-entropy FeCoNiCrCe LDH demonstrates the largest ECSA, which is beneficial for enhancing electrocatalytic activity. Roughness factor (R_f) is another performance parameter for evaluating the catalytic activity.[49] Since it can be obtained by dividing the by the geometric area of the working electrode, FeCoNiCrCe also exhibits the highest R_f. The higher ECSA and R_f are both conducive to the improved OER activity, as they favour the exposure of active sites. The change trend of these parameters is consistent with that of LSV, suggesting optimized conductivity and enriched active sites boost catalytic activity. Table S1 (SI) summarizes the catalytic performance parameters of the LDH electrodes prepared in this work. Moreover, FeCoNiCrCe exhibits superior OER activity and faster kinetics than lately reported electrocatalysts (Fig. 3f).

Stability is also an important criterion for assessing the efficiency of the catalysts,[6] and chronopotentiometric tests at 50 mA cm^{-2} were conducted on FeCoNiCrCe and FeCoNiCrCe-DC, respectively, to investigate the impact of the high-entropy stabilization effect. FeCoNiCrCe demonstrates remarkable stability during a 7-day test, with only a 0.2% potential increase. However, the FeCoNiCrCe-DC electrode exhibits a continuously rising voltage throughout the 48 h test, with a total increase of 0.13 V (Fig. 3g). Additionally, the electrolyte of FeCoNiCrCe-DC

turns green during the test, likely due to the Cr leaching.[11,15,54] The post-test OER activity of FeCoNiCrCe maintains 95.1% of its initial performance (Fig. 3h), confirming remarkable durability.

To summarize, FeCoNiCrCe exhibits superior OER performance to FeCoNiCrCe-DC, which can be attributed to the PC electrodeposition. The resulting surface of PC electrodeposition exhibits an optimized morphology with a uniform, near-equal element distribution, enabling more effective electronic modulation of the active sites by high-valence Cr and Ce in the local micro-region.[54] Moreover, the near-equal element content in FeCoNiCrCe is conducive to enhance configuration entropy, thereby exerting a favourable effect on its stability.[20] In contrast, although FeCoNiCrCe-DC prepared by DC electrodeposition possesses a higher Ni content, it shows inferior OER activity at high current densities and stability.

After the OER process, the surface morphology of FeCoNiCrCe and FeCoNiCrCe-DC was characterized. The surface construction of FeCoNiCrCe remains stable (Fig. 4a), which could attributed to excellent durability. However, the FeCoNiCrCe-DC (Fig. 4b) shows irregular aggregated particles and part of the NF substrate is exposed, suggesting morphology and catalytic activity degradation. The XPS test was also conducted after the OER test. The post-OER XPS survey spectrum of FeCoNiCrCe (Fig. S6) confirms retention of all five elements. Broadened XPS peaks (Fig. S7) reveal binding energy shifts: Fe 2p and Ni 2p shift to higher binding energies, while Co 2p move towards lower. Ce species transitions from a mixed Ce^{3+}/Ce^{4+} valence state to mono tetravalent. The increased oxidation states of metal ions promote the activation of oxygen ions and provide more active sites for the OER.[15] After the OER, the M–OH peak dominates the O 1s spectrum (Fig. 4c), suggesting the formation of (oxy)hydroxide on the surface of the FeCoNiCrCe electrode. The relative peak area ratio of –OH/M–O provides a rough assessment of the oxygen defect amount,[55] and the ratio of –OH/M–O exceeds that of the pristine material, indicating relatively more oxygen defects. Fig. 4d depicts the high-resolution Cr 2p spectra of FeCoNiCrCe and FeCoNiCrCe-DC after the OER. Compared to the spectra before the OER, the Cr element in both samples changes from Cr^{3+} (shown in Fig. 2d) to a mixed Cr^{3+}/Cr^{6+} state. Nevertheless, the signal intensity of Cr in the FeCoNiCrCe-DC indicates a loss of Cr during OER processes,[15,56] which is consistent with the observation that the electrolyte turned green during the stability test, while the content of Cr in FeCoNiCrCe remains stable. The construction of the high-entropy FeCoNiCrCe LDH prepared by PC electrodeposition can not only maintain an intact structure and morphology but also effectively restrain the loss of metal ions, thus offering a stable operation at a high current density.

4. Conclusions

The high-entropy FeCoNiCrCe LDH was *in situ* constructed on an NF substrate in just 20 minutes at room temperature *via* a facile and mild PC electrodeposition method as a high performance electrocatalyst for the OER. To comprehensively assess catalyst performance, systematic electrochemical evaluation was conducted. Key parameters such as overpotential, Tafel slope, charge transfer resistance, ECSA, roughness factor and mass activity were analysed. These insights provide a more detailed understanding of catalyst activity and efficiency for the OER. The FeCoNiCrCe LDH outperforms medium-/low-entropy

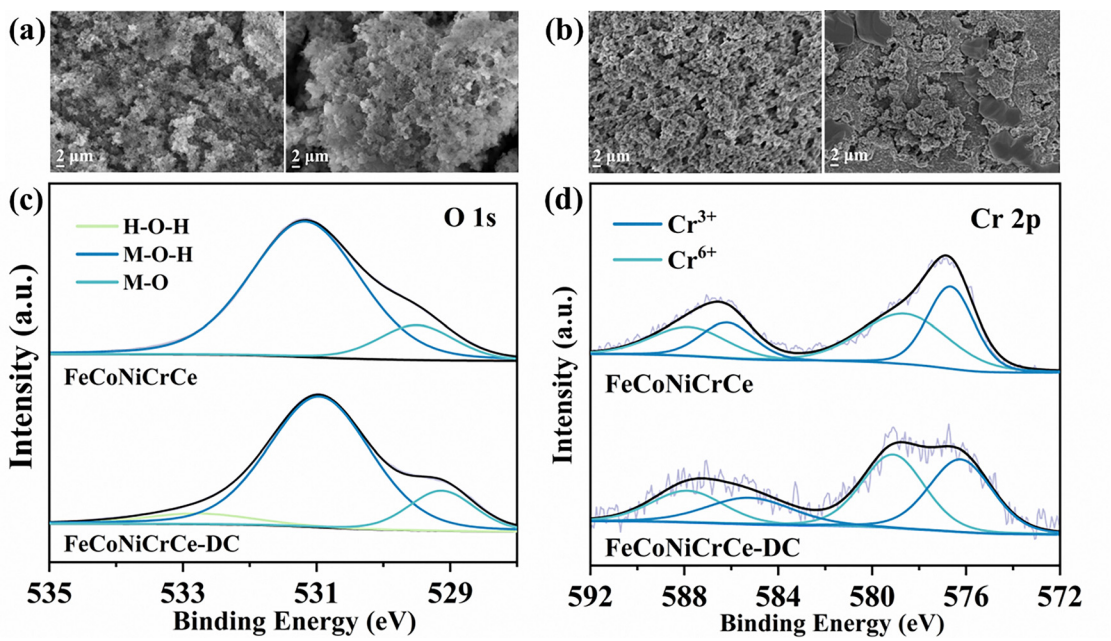

Fig. 4 Comparison of SEM images before (left) and after (right) the reaction of (a) FeCoNiCrCe of (b) FeCoNiCrCe-DC. High-resolution XPS spectra of (c) O 1s and (d) Cr 2p after the OER test.

LDHs obtained by the same method and the electrode prepared by the DC electrodeposition method, requiring the lowest overpotential across the tested range. It achieves a current density of 10 mA cm^{-2} with a low overpotential of 215 mV and a small Tafel slope of 45.15 mV dec^{-1}. Additionally, the overpotential remains low at 300 mV when the current density reaches 500 mA cm^{-2}, indicating its excellent catalytic activity for the OER at high current density. Notably, the FeCoNiCrCe demonstrates remarkable stability during a 7-day chronopotentiometric test at 50 mA cm^{-2}, with the required potential only increasing 0.2%. The enhancements arise not only from the coordination effects of five-metal composition, but more importantly, the PC-prepared electrode has a favourable microstructure compared with its DC counterpart. The FeCoNiCrCe with a crystalline/amorphous structure synthesized by the PC electrodeposition method exhibits optimized surface morphology and elemental composition, thus improving the conductivity and the exposure of active sites, enabling more effective electronic modulation of the active sites by Cr and Ce in the local micro-region. In contrast, despite the higher Ni content of FeCoNiCrCe-DC, it shows inferior OER activity under high current density and stability. The near-equal elemental content in FeCoNiCrCe is conducive to increasing the configuration entropy and amplifying the high-entropy stabilization effect, and thus inhibiting ion leaching compared to its DC counterpart, thereby leading to superior stability. This work reveals the microstructural advantages of PC electrodeposition, highlights the significance of uniform element composition and provides a feasible pathway for large-scale fabrication of high-entropy OER electrocatalysts with high performance.

Author contributions

Xinyu Yang: conceptualization, methodology, validation, data curation, and writing – original draft. Qianqiao Chen: methodology, validation, supervision, and funding acquisition.

Conflicts of interest

There are no conflicts to declare.

Data availability

The data supporting this article have been included as part of the article and its supplementary information (SI). Supplementary information: table S1, FTIR spectra, XRD patterns, XPS spectra and electrochemical test figures. See DOI: https://doi.org/10.1039/d5cp04024h.

Acknowledgements

This work was supported by the Top-notch Academic Programs Project of Jiangsu Higher Education Institutions and the Priority Academic Program Development of Jiangsu Higher Education Institutions.

References

1 Z. Hu, Q. Geng, S. Dong, M. Wang, Y. Song, W. Sun, H. Diao and D. Yuan, *J. Colloid Interface Sci.*, 2024, **671**, 34–45.
2 I. Khan, S. Khan, B. A. Alwan, A. E. Jery, M. Shayan, S. Wang, S. U. Hassan and M. Rizwan, *Small*, 2024, **20**, 2401034.
3 X. Ma, Y. Zhou, S. Zhang, W. Lei, Y. Zhao and C. Shan, *Small*, 2025, **21**, 2411394.
4 M. Tayebi, Z. Masoumi, M. Tayebi, B. Seo, C.-S. Lim, C. Hong, D. Kyung and H.-G. Kim, *ACS Appl. Energy Mater.*, 2025, **8**, 6677–6687.
5 M. Tayebi, Z. Masoumi, B. Seo, C.-S. Lim, C. Hong, H. J. Kim, D. Kyung and H. G. Kim, *ACS Appl. Mater. Interfaces*, 2024, **16**, 26107–26120.
6 Y. Liu, Q. Chen and Q. Zhong, *Nanoscale*, 2023, **15**, 14131–14139.
7 X. Yang, Y. Liu, Q. Chen, W. Yu and Q. Zhong, *Langmuir*, 2024, **40**, 24605–24612.
8 M. Tayebi, Z. Masoumi, H. Lee, D. Hong, B. Seo, C.-S. Lim, D. Kyung and H.-G. Kim, *Adv. Sustainable Syst.*, 2024, **8**, 2400342.
9 W. Dong, Q. Pan, Z. Liu, H. Sun, Z. Shi and J. Xu, *Int. J. Hydrogen Energy*, 2023, **48**, 35493–35501.
10 S. L. Fereja, Z. Zhang, Z. Fang, J. Guo, X. Zhang, K. Liu, Z. Li and W. Chen, *ACS Appl. Mater. Interfaces*, 2022, **14**, 38727–38738.
11 T. X. Nguyen, Y. H. Su, C. C. Lin and J. M. Ting, *Adv. Funct. Mater.*, 2021, **31**, 2106229.
12 Y. Wan, W. Wei, S. Ding, L. Wu and X. Yuan, *Small*, 2024, **20**, 2404689.
13 Y. Liu, Y. Ying, L. Fei, Y. Liu, Q. Hu, G. Zhang, S. Y. Pang, W. Lu, C. L. Mak, X. Luo, L. Zhou, M. Wei and H. Huang, *J. Am. Chem. Soc.*, 2019, **141**, 8136–8145.
14 X. Yang, R. Guo, R. Cai, Y. Ouyang, P. Yang and J. Xiao, *Int. J. Hydrogen Energy*, 2022, **47**, 13561–13578.
15 D. Wang, C. Duan, Y. Yu, X. Li, Z. Wang, Y. Liu and C. Liu, *J. Alloys Compd.*, 2023, **967**, 171758.
16 J. Xing, Y. Liu, G. Mathew, Q. He, J. Aghassi-Hagmann, S. Schweidler and B. Breitung, *Adv. Sci.*, 2025, **12**, 2411175.
17 Y. Ding, Z. Wang, Z. Liang, X. Sun, Z. Sun, Y. Zhao, J. Liu, C. Wang, Z. Zeng, L. Fu, M. Zeng and L. Tang, *Adv. Mater.*, 2023, **37**, 2302860.
18 X. Chu, T. Wang, H. Wang, B. Du, G. Guo, Y. Zhou and X. Dong, *J. Alloys Compd.*, 2024, **1003**, 175584.
19 D. Liu, X. Yan, P. Guo, Y. Yang, Y. He, J. Liu, J. Chen, H. Pan and R. Wu, *ACS Catal.*, 2023, **13**, 7698–7706.
20 S. Li, L. Tong, Z. Peng, B. Zhang and X. Fu, *J. Mater. Chem. A*, 2023, **11**, 13697–13707.
21 T. X. Nguyen, C. C. Tsai, V. T. Nguyen, Y.-J. Huang, Y.-H. Su, S.-Y. Li, R.-K. Xie, Y. J. Lin, J. F. Lee and J.-M. Ting, *Chem. Eng. J.*, 2023, **466**, 143352.
22 F. Wang, P. Zou, Y. Zhang, W. Pan, Y. Li, L. Liang, C. Chen, H. Liu and S. Zheng, *Nat. Commun.*, 2023, **14**, 6019.
23 C. Deng, R. Liu, P. Wu, T. Wang, S. Xi, D. Tao, Q. He, Y. Chao, W. Zhu and S. Dai, *Small*, 2024, **20**, 2406685.
24 Z. Zhu, Y. Zhang, D. Kong, N. He and Q. Chen, *Small*, 2024, **20**, 2307754.

25 Z. Sun, A. Curto, J. Rodriguez-Fernandez, Z. Wang, A. Parikh, J. Fester, M. Dong, A. Vojvodic and J. V. Lauritsen, *ACS Nano*, 2021, **15**, 18226–18236.
26 H. Bian, P. Qi, G. Xie, X. Liu, D. Zhang and P. Wang, *Chem. Eng. J.*, 2023, **477**, 147286.
27 M. Li, X. Wang, K. Liu, Z. Zhu, H. Guo, M. Li, H. Du, D. Sun, H. Li, K. Huang, Y. Tang and G. Fu, *Adv. Energy Mater.*, 2023, **13**, 2301162.
28 Y. Li, X. Zhang and Z. Zheng, *Small*, 2022, **18**, 2107594.
29 C.-S. Ni, S.-F. Liu, J.-F. Lee, C.-W. Pao, J.-L. Chen, H.-Y. Chen and J.-H. Huang, *Electrochim. Acta*, 2021, **384**, 138415.
30 H. Bian, R. Wang, K. Zhang, H. Zheng, M. Wen, Z. Li, Z. Li, G. Wang, G. Xie, X. Liu and L. Jiang, *Surf. Coat. Technol.*, 2023, **459**, 129407.
31 C.-Z. Yao, P. Zhang, M. Liu, G.-R. Li, J.-Q. Ye, P. Liu and Y.-X. Tong, *Electrochim. Acta*, 2008, **53**, 8359–8365.
32 X. G. Chen, X. Zhao, Y. Y. Wang, S. S. Wang, Y. Y. Shang, J. Xu, F. M. Guo and Y. J. Zhang, *ChemCatChem*, 2021, **13**, 3619–3627.
33 G. F. N. Freitas, W. S. Gomes, J. P. I. Souza, C. N. Pinotti, E. C. Passamani, M. F. Montemor and R. Della Noce, *Mater. Chem. Phys.*, 2023, **309**, 128438.
34 Y. Zhang, Y. Zhong, Y. Yu, M. Wang and Z. Guo, *J. Electrochem. Soc.*, 2024, **171**, 063504.
35 Z. Zhu, H. Meng and P. Ren, *Colloids Surf., A*, 2022, **648**, 129404.
36 Z. Shojaei, G. R. Khayati and E. Darezereshki, *Int. J. Miner., Metall. Mater.*, 2022, **29**, 1683–1696.
37 S.-Q. Chang, C.-C. Cheng, P. Y. Cheng, C.-L. Huang and S.-Y. Lu, *Chem. Eng. J.*, 2022, **446**, 137452.
38 Y. Sun, T. Tang, L. Xiao, J. Han, X. Bai, M. Shi, S. Chen, J. Sun, Y. Ma and J. Guan, *Chem. – Eur. J.*, 2024, **30**, e202303779.
39 R. Zhou, X. Han, Q. Chen, L. Peng, X. Qiu, P. Wang, C. Guo, J. Wang, Z. Wang and J. Hao, *J. Mater. Chem. A*, 2024, **12**, 5719–5730.
40 Y. Gan, Y. Ye, X. Dai, X. Yin, Y. Cao, R. Cai, B. Feng, Q. Wang, Y. Wu and X. Zhang, *J. Colloid Interface Sci.*, 2024, **658**, 343–353.
41 Y. Liao, R. He, W. Pan, Y. Li, Y. Wang, J. Li and Y. Li, *Chem. Eng. J.*, 2023, **464**, 142669.
42 Z.-L. Wang, G.-Y. Huang, G.-R. Zhu, H.-C. Hu, C. Li, X.-H. Guan and H. B. Zhu, *Appl. Catal., B*, 2025, **361**, 124585.
43 B. Wang, X. Wu, S. Jia, J. Tang, H. Wu, X. Wang, S. Gao, H. Li, H. Lu, G. Fu, X. Meng and S. Tang, *J. Mater. Sci. Technol.*, 2025, **227**, 255–261.
44 L. Zhao, M. Hong, X. Zhang, C. Du and J. Chen, *J. Alloys Compd.*, 2025, **1016**, 179010.
45 L. Yao, H. Zhang, M. Humayun, Y. Fu, X. Xu, C. Feng and C. Wang, *J. Alloys Compd.*, 2023, **936**, 168206.
46 C. Wang, R. Wang, Y. Peng, J. Chen and J. Li, *Chem. Commun.*, 2019, **55**, 10944–10947.
47 H. Xu, Y. Liao, Z. Gao, Y. Qing, Y. Wu and L. Xia, *J. Mater. Chem. A*, 2021, **9**, 3418–3426.
48 Y. Liu, C. Li, C. Tan, Z. Pei, T. Yang, S. Zhang, Q. Huang, Y. Wang, Z. Zhou, X. Liao, J. Dong, H. Tan, W. Yan, H. Yin, Z.-Q. Liu, J. Huang and S. Zhao, *Nat. Commun.*, 2023, **14**, 2475.
49 M. Asim, A. Hussain, S. Kanwal, A. Ahmad, Y. Aykut, A. Bayrakçeken and N. K. Janjua, *Mater. Adv.*, 2024, **5**, 8490.
50 S. Kanwal, A. Kanwal, A. Dawood, M. H. Nasir, A. Hussain, M. Asim, F. Benabdallah and N. K. Janjua, *Ionics*, 2025, **31**, 2439–2456.
51 W. Shen, Y. Du, H. Liu, C. W. Tsang, X. Chen and C. Liang, *Small*, 2024, **20**, 2404379.
52 G. M. Tomboc, T. Kwon, J. Joo and K. Lee, *J. Mater. Chem. A*, 2020, **8**, 14844–14862.
53 M. Asim, A. Hussain, S. Kanwal, M. Samancı, A. Bayrakçeken, A. S. Fedorkova and N. K. Janjua, *J. Alloys Compd.*, 2025, **1016**, 178967.
54 X. Huang, L. Xiao, C. Han, W. Zhang, Y. Liu, J. Zhang, H. Tan, R. Zhang, P. Yin, C. Dong, H. Liu and X. Du, *Int. J. Hydrogen Energy*, 2025, **140**, 187–193.
55 L. Wu, L. Yu, Q. Zhu, B. McElhenny, F. Zhang, C. Wu, X. Xing, J. Bao, S. Chen and Z. Ren, *Nano Energy*, 2021, **83**, 105838.
56 B. Feng, J. Chen, Y. Yang, C. Zhong, X. Zhao and Y. Yao, *J. Materiomics*, 2024, **10**, 919–927.

